J Nanopart Res (2019) 21: 208
https://doi.org/10.1007/s11051-019-4634-y

RESEARCH PAPER

Agglomeration of iron oxide nanoparticles: pH effect is stronger than amino acid acidity

Anna Godymchuk · Iuliia Papina · Elizaveta Karepina · Denis Kuznetsov · Ivan Lapin · Valery Svetlichnyi

Received: 16 March 2019 / Accepted: 13 August 2019 / Published online: 2 October 2019

Abstract Wet methods for nanoparticle characterization need to use the surfactants to prevent the agglomeration of particles in hydrosols. In this work, we investigated the effect of pH on the agglomeration state and the stability of differently sized Fe_2O_3 nanoparticles, notably 35 and 120 nm in average, in amino acid solutions as glycine, L-lysine and L-glutamine, using the method of dynamic light scattering. The lowest electrokinetic stability and maximum agglomeration of both hydrosols was found in the acidic medium, particularly, at pH = 3.5 for Fe_2O_3-35 and pH = 6.5 for Fe_2O_3-120 (surface isoelectric point). At pH ≤ 7 in amino acid–based solutions, the charge direction was depended on the particles size. The pH growth from 5 to 9 suppressed Fe_2O_3 particle agglomeration although the effect of pH was much higher in glycine (neutral amino acid) where the agglomerates' size decreased by 4.5 times compared with 2.8 in glutamine (acidic amino acid) and 1.8 in lysine (basic amino acid). It was concluded that the pH predominantly affected an agglomeration with respect to the particle size and acidity of amino acids. In alkali medium at pH = 9, particles had a maximum charge and minimum size in all solutions. For example, in glycine, the average size/zeta potential of Fe_2O_3-35 and Fe_2O_3-120 agglomerates were, respectively, 180 ± 20 nm/− 32 mV and 263 ± 80 nm/− 38 mV compared with water 510 ± 20 nm/− 18 mV and 180 ± 69 nm/− 24 mV.

Keywords Nanoparticles · Iron oxide (III) · Amino acid · Glycine · Lysine · Glutamic acid · Hydrosol · Agglomeration · pH · Zeta potential · Average size · Dynamic light scattering · Hematite

A. Godymchuk · I. Papina · E. Karepina
National Research Tomsk Polytechnic University, 30 Lenina Avenue, Tomsk, Russia 634050

A. Godymchuk (✉)
Tobolsk Complex Scientific Station, Ural Branch of the Russian Academy of Science, 15 Osipov Academician Street, Tobolsk, Russian Federation 626152
e-mail: godymchuk@tpu.ru

D. Kuznetsov
National University of Science and Technology "MISiS", 4 Leninsky Avenue, Moscow, Russia 119049

I. Lapin · V. Svetlichnyi
National Research Tomsk State University, 36 Lenina Avenue, Tomsk, Russia 634050

Introduction

Iron oxide nanoparticles (IONPs) are widely demanded in diverse engineering sectors because of their improved magnetic, optical, catalytic, electrochemical, and thermophysical properties. IONPs with controlled particles surface, chemical composition, shape, and size, are used as catalysts (Nagajyothi et al. 2017). They have great potential as contaminant removal (Parida et al. 2017; Gao et al. 2016), remediation, and water treatment (Mohammed et al. 2017). Due to their high biocompatibility, low toxicity, and spatial imaging capability, IONPs with an appropriate surface chemistry can be beneficial in nanotheranostic application for cancer imaging and treatment (Ren et al. 2014; Bao et al. 2015). Thus, an

extensive application of IONPs results in the unprecedented growth of their elaboration and production.

For a better understanding of nanoparticle behavior and control of their properties, whole life cycle of nanoscaled particles is inevitably accompanied with the characterization of particle size (Holbrook et al. 2015; Cabrera et al. 2015). Scientists use various methods for size analysis such as transmission electron microscopy, laser diffraction, mass-spectrometry with inductively coupled plasma, low-temperature adsorption of nitrogen, and nanoparticle tracking analysis (Rasmussen et al. 2018). Although each method has advantages, dynamic light scattering (DLS) is often chosen by specialists since it is highly expressed and cheap method which allows fast measurements (Ramos 2017).

Despite the effectiveness of the DLS method, it requires the use of nanoparticles dispersed in a liquid, most often in an aqueous medium. Compared with stirring and sonication used to disperse particles (Farre et al. 2009), the application of stabilizers is preferable to control the size growth of IONPs in liquids for a long time (Bhattacharya et al. 2011; Li et al. 2017; Jiang et al. 2009).

Amino acids exhibit environmentally favorable characteristics, such as green, low irritation, good antibacterial properties, excellent water solubility, and biodegradability (Doyen et al. 2016). Moreover, amino acids possess unique zwitterionic nature due to the presence of amine and carboxylic groups, which can both be used for nanoparticle surface functionalization depending on the conditions (Shen et al. 2017). Therefore, amino acids (e.g,. glycine (Chaudhari et al. 2013; Biju et al. 2014), L-phenylalanine, L-serine, L-alanine, L-glutamine, L-glutamic acid (Kandori et al. 2006; Wang et al. 2011), L-aspartic acid, L-lysine, L-asparagine (Wang et al. 2011), and L-arginine (Cao et al. 2008)) have been widely used as assistants for the fabrication and modification of differently shaped IONPs (Li et al. 2017). Besides, proteins, drugs, and other biomolecules can be attached through the surface amino group (Mohapatra et al. 2007). Thus, amino acids help to simulate biological media directly during dispersive analysis.

On the other hand, the charge and the size of IONPs stabilized entirely by electrostatic repulsion are highly sensitive to pH fluctuation (Lin et al. 2005; Lin et al. 2018; Teja and Koh 2009). It has been reported that after coating with citric acid, the zeta potential of IONPs was − 35 mV compared with bare IONPs (− 8 mV) at pH = 7. But the surface isoelectric point of coated IONPs was close to pH = 3 (De Sousa et al. 2013). There are studies (Ingram et al. 2010; Li et al. 2014; Morgan et al. 1986), where the oleic acid may show improved colloidal stability at neutral and basic pH conditions and prevents rapid agglomeration under slightly acidic pH conditions (pH = 5). Bare magnetite nanoparticles, with an isoelectric point close to neutral pH, are not very stable and can easily agglomerate in natural aquatic systems (Liu et al. 2008).

When controlling the pH of the medium, it is possible to fabricate nanocomposites of nanographene-doped Fe_2O_3 with a larger specific surface area by introducing acidic amino acid. However, it was shown that the composites prepared by adding basic (lysine) and neutral (glycine) amino acids were agglomerated and had smaller surface area (Wu et al. 2018). Other authors have demonstrated that an increase of the pH may have an adverse effect on IONP dispersions containing functional groups. Indeed, at pH growth from 4 to 9, functionalization by NH_2- and SH- groups causes the agglomeration of chitosan-coated magnetic nanoparticles compared with OH- and COOH- ions that lead to strong disagglomeration (Bhattacharya et al. 2011).

It was also shown that the adsorption efficiency of alginate on γ-Fe_2O_3 was increased at high pH values due to strong electrostatic interactions between carboxylate functions of alginate and cationic dye (Talbot et al. 2018). However, the adsorption amounts of alginate on Fe_3O_4 nanoparticles decreased with increasing pH, and the zeta potential of alginate-coated Fe_3O_4 nanoparticles shifted to a lower value but remained to be positive at lower pH (Xu et al. 2006). It was clearly demonstrated that the functionalization of magnetic nanoparticles with cysteine could be done only under acidic conditions (pH = 4–5) (Kast and Schnurch 2001; Schnurch et al. 2004). Furthermore, α-amino acids such as glycine, lysine, serine, and glutamic acid, showed trends of different absorptions onto engineered TiO_2 nanoparticles in buffered solutions at pH of 6, 7.4, and 9 (Ustunol et al. 2019). The differences were attributed to the different speciation of the functional groups within the amino acids and the TiO_2 surface charge at each pH.

Although the value of pH is crucial for synthesizing and stabilizing nanoparticles, the choice of the amino acid as a surfactant for IONPs is still questionable since their acidity determines the surface chemistry and

thereby particles' agglomeration and stability. There is still lack of results demonstrating the difference between acidity of amino acids used for stabilizing IONPs at the broad range of pH. Moreover, the size and surface charge of engineered nanoparticles are of great concern in terms of understanding particles' migration in living organisms. Due to the diversity of engineered nanoparticles, the accumulation of experimental data is still necessary to develop methods for preparing hydrosols with high agglomeration stability.

The purpose of this work was to show the effect of the pH, the acidity of low molecular weight aliphatic amino acids, and the size of nanoparticles on the agglomeration state and stability of iron oxide nanoparticles in a hydrosol.

Materials and methods

Engineered nanoparticles

We used two batches of IONPs labeled as Fe_2O_3-35 and Fe_2O_3-120. The sample of Fe_2O_3-35 was obtained via 4-h annealing of Fe_3O_4 nanoparticles at 500 ± 0.5 °C in a muffle furnace SNOL 6.7/1300 (Lithuania, heating rate—10 °C/min) prior to a natural cooling until 25 ± 2 °C. Initial Fe_3O_4 nanoparticles were synthesized by pulsed laser ablation of iron target (99.5% of Fe) in air by laser with wavelength of 1064 nm, pulse duration of 7 ns, repetition frequency of 20 Hz, and laser pulse energy of 150 mJ (the pulse density of the radiation power density of 400 MW/cm^2). The experimental conditions on laser ablation and the characteristics of the nanoparticles for the sample of Fe_2O_3-35 are given in detail in (Svetlichnyi et al. 2018). The sample Fe_2O_3-120 was obtained by electrical explosion of iron wire in air atmosphere and was purchased from Advanced Power Technologies LLC, Tomsk, Russia.

Characterization of dry nanoparticles

The specific surface of IONPs was determined by low-temperature adsorption of nitrogen (BET method) using a NOVA 1200e device (Quantachrome Instr., USA, error—± 0.20 m^2/g). The obtained surface value was used to calculate the surface average diameter of particles (d_S), assuming that all the particles had the same diameter and a spherical shape by the formula:

$d_S = \frac{6}{\rho \cdot S}$, where d_S was surface average diameter of particles (m); S is the specific surface of particles (m^2/kg); ρ is the matter density (kg/m^3) (5.24 for Fe_2O_3).

The phase composition of IONPs was identified by the powder X-ray diffraction on a diffractometer XRD-7000 (XRD, Shimadzu, Japan). The X-ray record was performed using the CuK_α-emission in 2θ angles ranging from 10 to 70°. Decryption was performed by card index of ICPDS (International Center for Diffraction Date).

The morphology of nanoparticles was determined by a scanning electron microscope VEGA3 (SEM, Tescan, Czech Republic). Before recording, a carbon film was sputtered on a thin layer of powder, applied on a conductive tape; recording was carried out at an accelerating voltage of 0.1–30 kW.

Surfactants

Three aliphatic amino acids of different acidities were used as stabilizers of particles: amino acetic acid (Gly, glycine, NH_2-CH_2-COOH, CAS 56-40-6, neutral amino acid), L-glutamic acid (Glut, $C_5H_9NO_4$, CAS 56-85-9, acidic amino acid), and L-lysine (Lys, $C_6H_{14}N_2O_2$, CAS 56-87-1, basic amino acid) produced by Sigma-Aldrich. Amino acids possess unique zwitterionic nature due to the presence of both amine and carboxylic groups. Due to two COOH groups, Glut is an acidic hydrophilic acid, and due to two NH_2 groups, lysine is a basic hydrophilic acid. For all selected pH, these amino acids behave either as acids (proton donors) or as bases (proton acceptors). From the studied pH range (3–9), we excluded the isoelectric points of amino acids (3.24—Glut, 5.97—Gly, 9.82—Lys) since at these pH values, acids' hydrophilicity was low. However, based on acids' isoelectric points, we can suggest that dissolved Gly does not form charged particles (non-ionic surfactant), Glut is a source of H^+ and forms an anion (anionic surfactant), and Lys is a protonated acid in water carrying a positive charge in aqueous solutions (cationic surfactant).

Considering the broad pH range of natural and engineered aquatic environments (5–9), it is important to study the stability of IONPs over this pH range. However, in most of previous studies, the stability of organic-coated IONPs was only studied at neutral pH condition (Majewski and Thierry 2007; Tartaj et al. 2003; Teja and Holm 2002).

Preparation of surfactant solutions

In all manipulations, we used distilled water with pH = 6.3–6.9, obtained on a D-30938 distiller (Gesellschaft Labortechnik mbH). The pH value was controlled with a pH meter pH-150MI (Izmeritelnaya technika, Russia). Samples of nanoparticles and substances were prepared with the AND GR-202 scales (A&D Co Ltd., Japan, ± 0.0001 g). The stirring of solutions and the titration was performed with a magnetic stirrer MR Hei-Tec (Heidolph Instruments GmbH & Co, Germany) at the frequency of 300 cycles per minute (the magnetic bar with size of 5 × 10 mm). All solutions and suspensions were prepared and stored at 25 ± 2 °C.

The solutions of surfactants with a concentration of 0.05 wt% were prepared based on distilled water in glass vessels (100 ml). The Glut solution was alkalified in a molar ratio of NaOH:Glut = 1:1 until complete dissolution. Prepared solutions of Gly, Lys, and Glut with pH 6.7, 9.8, and 6.5, respectively, were kept for no more than 24 h; after which, the pH was adjusted to pH = 3, 5, 7, and 9 by titration with 0.1 M NaOH, and 0.1 M HNO_3.

Preparation of nanoparticle suspensions

Nanoparticle hydrosols were prepared based on distilled water adjusted to the predetermined pH in plastic containers (50 ml). The concentration of the particles in the solution was adjusted experimentally to obtain reproducible results on a laser diffractometer and was 0.01 and 0.1 wt% for Fe_2O_3-35 and Fe_2O_3-120 hydrosols, respectively. Hydrosols were mixed by vortexing and incubated at most 24 h.

To prepare a hydrosol, a dry amino acid was mixed with dry nanoparticles in a plastic container of a homogenizer Ultra-Turrax Tube Drive (IKA, Germany) with glass beads (diameter of 5 mm) by shaking with a power of 5 units (speed of 3300 rpm). Components were mixed within 3 min prior to a gradual adding of 1, 4, 5, and 40 ml of surfactant solution with the predetermined pH and alternate shaking on a homogenizer for 3 min after each addition. Mixing dry nanoparticles with dry acids provided more even distribution of a stabilizer on the particles surface due to the absence of OH ions tending to the surface in water surrounding.

The final hydrosols were again adjusted to the required pH by titration of 0.1 M NaOH, and 0.1 M HNO_3. The mass ratio of the NP:acid was 1:1. Next, the hydrosols were separated from the beads with a polymer sieve followed by the sonication on a UIP1000hd ultrasonic homogenizer (Transducer, Germany, 1000 W, 20 kHz) for 1 min. Sampling for analysis was carried out at least three times within 24 h from the upper third of the volume of the hydrosols after shaking for 1 min.

We prepared fresh suspensions for each experiment. The experiment was repeated at least three times in different days at 25 ± 0.5 °C.

Characterization of hydrosols

The agglomeration state and stability of particles were evaluated based on the measurement of quantitative particle size distribution (PSD) and zeta potential (ZP) of particles in hydrosols. The measurements were taken by dynamic light scattering technique, based on the Smoluchowski calculations, by a Zetasizer nanoparticle analyzer equipped with the helium-neon laser with 4-mV power and 633-nm wavelength (Malvern, USA).

To calculate statistics, we took reproducible data conforming to ISO standards. The selection of experimental result was carried out according to quality criteria parameters of the instrument. During each measurement, the mean counting rate of scattering light reported was between 100 and 500 counts per seconds. The instrument attenuator value was between 4 and 9. For routinely analysis, T was set at 25 °C. Triplicate measurements were taken with 120-s equilibrium time between each repetition. The measurement quality was evaluated by the correlation function and count rate plot considering the polydispersity and sedimentation of the system and the phase plot for measuring zeta potential (ISO 13099-2: 2012). The U-shaped polystyrene cuvette was used for measurements.

Electrostatic mobility of particles was used to determine the zeta potential, and the calculated results depended on various conditions such as nanomaterial properties, solution features, and the selected theoretical model. The Smoluchowski model was applied to measure the zeta potential of nanoparticles and their agglomerates by the following equation:

$$\zeta = \mu \cdot \eta / (\varepsilon_0 \cdot \varepsilon_r),$$

where μ is the electrostatic mobility, $\eta = 8.90 \cdot 10^{-4}$ (Pa s) is the viscosity of the solvent (water, 25 °C), $\varepsilon_0 = 8.85$ (pF/m) is the vacuum permittivity, and $\varepsilon_r = 78.54$ (pF/m) is the relative permittivity of water.

The quantitative particle size distribution was used to calculate an average particle size (d_{av}) according to the formula:

$d_{av} = \sum d \frac{q\ (\%)}{100\ (\%)}$, where d represented the particle size in dispersion, and q is the differential percent of particles with the size d in the dispersion.

Results and discussion

Nanoparticle composition and morphology

According to XRD, nanoparticle phase composition preferably comprises phase of hematite (α-Fe_2O_3, Fig. 1). The sample Fe_2O_3-120 contains residual amounts of Fe_3O_4 and Fe (Table 1). The nanopowders are nearly similar in shape (Fig. 2a and b), but they have a different dispersion compositions and specific surface. The average particle size of Fe_2O_3-120 calculated from BET method is consistent with SEM analysis (Table 1). For Fe_2O_3-35, a bigger BET particle size is due to the partial fusion between particles.

SEM images show that primary particles form agglomerates (Fig. 2) with average sizes of 239 and 659 nm—on average 6.8 and 5.5 particles in an agglomerate, respectively, for Fe_2O_3-35 and Fe_2O_3-120 (Table 1).

pH effect on particle agglomeration in hydrosols

When entering an aqueous medium, particle agglomerate and and the particle size distribution (PSD) for Fe_2O_3-35 is 90–3000 nm (SEM 23–447 nm) (Fig. 3), and for Fe_2O_3-120 is 79–1990 nm (SEM 85–1204 nm) (Fig. 4). In Fe_2O_3-35 hydrosols at pH = 3, we can see the bimodal PSD with the modes of 190 nm (q_1 = 12%) and 460 nm (q_2 = 7%, Fig. 3a), whereas at pH = 5, the modes are 255 (q_1 = 10%) and 531 nm (q_2 = 9%, Fig. 3b) and at pH = 9, there is a monomodal PSD with a peak of 342 nm (q = 13%, Fig. 3d). In a neutral medium, we find trimodal PSD with the modes of 255 (q_1 = 9%), 460 (q_2 = 8%), and 1281 nm (q_3 = 5%, Fig. 3c). Besides, at pH = 7, there is the highest measurement error characterized by a high instability of resulting systems. It is noted that the maximum peak of PSD obtained at the pH of 3, 5, 7, and 9 on the size scale moves to the right and is related to the size of 190, 255, 255, and 342 nm (Fig. 3).

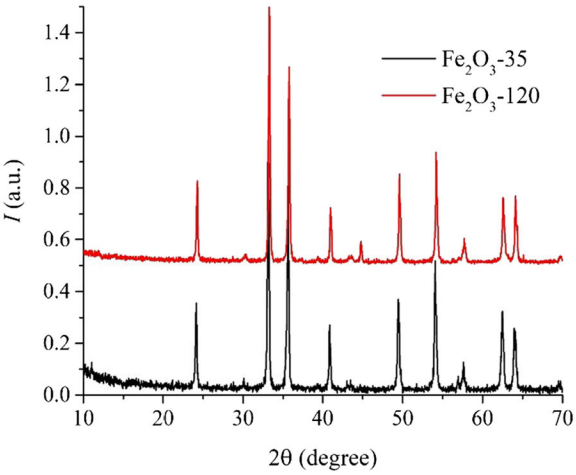

Fig. 1 XRD patterns of nanoparticles

Regardless of the medium acidity, the PSD of Fe_2O_3-120 particles remains bimodal, but the mode values change randomly (Fig. 4). In general, with increasing pH, PSDs are shifted to the left and are 142–2670 nm (Fig. 4a), 106–1280 nm (Fig. 4b), 122–484 nm (Fig. 4c), and 79–1100 nm (Fig. 4d) for hydrosols with pH 3, 5, 7, and 9, respectively. It has been found that at pH = 3, the mode of the largest peak is 342 nm (20% in Fig. 4a); in an alkaline medium, most of the particles in water (28%) have a size of 106 nm (Fig. 4d).

The analysis of the obtained distributions has shown that all hydrosols contain both individual and agglomerated particles not divided under sonication. In this case, it is possible to generalize the pH effect on the agglomeration stability by comparison of the average particle size (d_{av}) and zeta potential (ZP).

The agglomeration stability of Fe_2O_3-35 hydrosols noticeably lessens and the surface is positively charged at lower pH: with the increasing pH from 3 to 5, d_{av} goes up from 318 ± 30 to 565 ± 80 nm (Fig. 5a), and the ZP decreases from + 35 to + 17 mV (Fig. 5b). In the pH range of 5–9, the lowest electrokinetic stability of suspensions is observed: the absolute value of the ZP does not exceed 17 mV (Fig. 5b), and d_{av} is 545 ± 45 nm (Fig. 5a). The surface of Fe_2O_3-35 is charged neutrally at pH = 6.5. Contrary, rhomb-shaped α-Fe_2O_3 particles with sizes 28 × 39 nm had zero charge at pH = 8.2 measured by potentiometric titration (Demangeat et al. 2018). Although 10-nm Fe_3O_4 particles with aggregates of 205.7 nm had an isoelectric point near to pH = 6.8 (Favela-Camacho et al. 2019), bare Fe_3O_4 particles with size of 9.3 nm was charged positively in the pH range between 3 and 9 (Xu et al. 2006). Differently,

Table 1 Composition and morphology of the studied nanoparticles

Sample	XRD	BET	SEM	
	Phase composition	Specific surface, m^2/g/average particle size (nm)	Size distribution/average particle size (nm)	Size distribution/average size of primary agglomerates (nm)
Fe_2O_3-35	Fe_2O_3	19.2/59.6	23–150/35	125–447/239
Fe_2O_3-120	Fe_2O_3 92% Fe_3O_4 4% Fe 4%	9.8/114.5	85–218/120	252–1204/659

chemically synthesized γ-Fe_2O_3 nanoparticles with a median diameter of 12 nm at neutral pH approach the value of zero-charge determined from acoustophoresis during titrations (Lucas et al. 2007).

In our findings, the best electrokinetic stability was observed at pH = 3 that agrees with the results showing relatively high colloidal stability of γ-Fe_2O_3 particles which at pH = 3 had the ZP + 20 mV (Lucas et al. 2007). Also, at pH = 6 and lower, the pH drastically modified the α-Fe_2O_3 size distribution to a more stable aggregation state characterized by a monomodal distribution (40 nm) and higher abundance of finer particles (< 400 nm) in (Demangeat et al. 2018).

Regarding Fe_2O_3-120, the surface charge exchange at pH = 3.5 weakly affects the particle agglomeration state: at pH 3–4 the value of d_{av} is fluctuating within the range of 320–344 nm (Fig. 5a). Despite the maximum electrokinetic stability of Fe_2O_3-120 in neutral and weakly acidic media (ZP is 21–− 25 mV, Fig. 5b), the size of the agglomerates has the highest value (520 ± 213–580 ± 314 nm, Fig. 5a). When adding H^+ or OH^- ions, the d_{av} reduces to 385 ± 122 (pH = 5) and 177 ± 103 nm (pH = 9, Fig. 5a), although ZP value varies insignificantly (− 18–− 20 mV) in the range of pH = 5–9 (Fig. 5b).

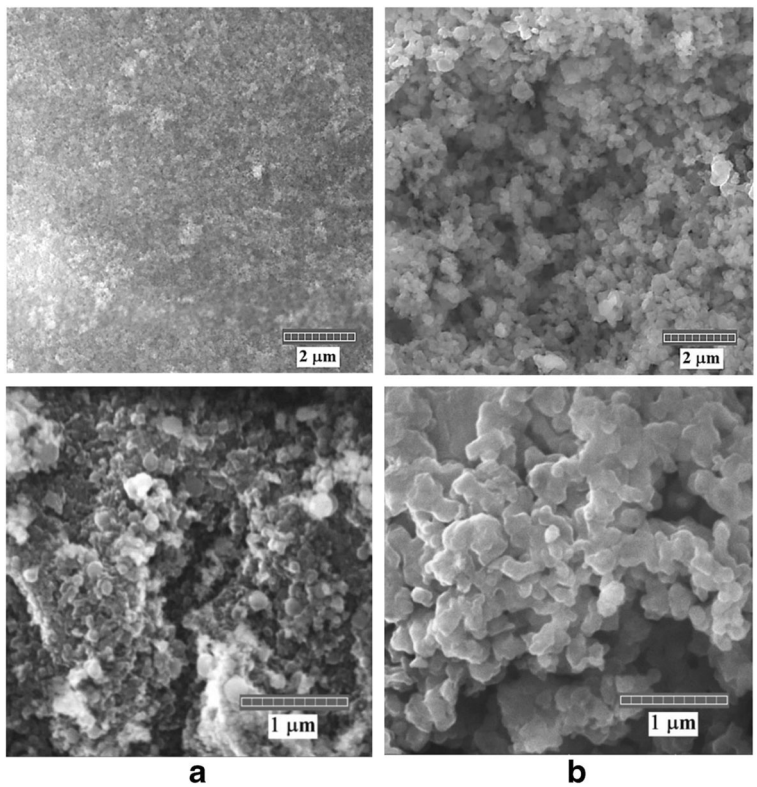

Fig. 2 SEM images of nanoparticles: Fe_2O_3-35 (**a**) and Fe_2O_3-120 (**b**)

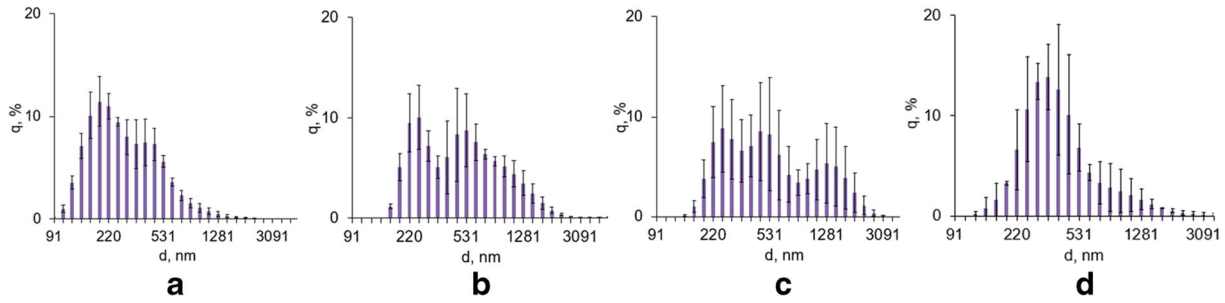

Fig. 3 The particle and agglomerate size distribution for Fe_2O_3-35. **a** pH = 3. **b** pH = 5. **c** pH = 7. **d** pH = 9

In general, with pH increasing from 3 to 9, Fe_2O_3-35 nanoparticles tend to agglomerate more while Fe_2O_3-120 better resists agglomeration. Herewith, disregarding the dry particles' size, the fewest probability of IONP agglomeration has been found in acidic and neutral media. It has also been noted that the decrease of the particle size from 120 to 35 nm leads to a shift of the surface isoelectric point from pH = 3.5 to pH = 6.5.

pH effect on the particle agglomeration in surfactant solutions

Acid-basic conditions have a great influence on the agglomeration state and stability of IONP hydrosols. According to DLS, both particles agglomerate in surfactants at high acidity: for example, at pH = 3, the average sizes of agglomerates for Fe_2O_3-35 and Fe_2O_3-120 are 2.0 ± 0.2 (Fig. 6a) and 3.0 ± 0.5 times (Fig. 7a) higher in average in comparison with water. With the increase of pH from 5 to 9, the d_{av} value is predominantly reduced in all amino acids: for example, in the Glut at pH 5, 7, and 9, the d_{av} values of Fe_2O_3-35 and Fe_2O_3-120 are 480, 200, and 170 nm (Fig. 6a) and 1065, 1058, and 370 nm (Fig. 7a), respectively. Therefore, the disagglomeration of particles in surfactants becomes more perceptible in a neutral medium, and with an excess of OH^- ions (pH = 9), the size of agglomerates is the lowest. The disagglomeration may be due to the adsorption of amino acids in the form of $H_2N\text{-}CHR\text{-}COO^-$ anions in an alkaline medium, which compete with OH^- ions and concentrate near particle surface forming a thick diffusive layer of counter-ions.

Dispersion properties of the particles in amino acid solutions correspond to the electrokinetic state of their surface. Adding an amino acid shifts the pH of isoelectric point for the Fe_2O_3-35 from 6.5 to 3.8–4.2, and for Fe_2O_3-120 from 3.5 to 5. In the hydrosols of Fe_2O_3-120 at pH = 3–5, the most unstable suspensions are formed and the absolute value of ZP was less than 18 mV. It has been shown that the ZP value is lower for higher pH conditions (the surface becomes more negatively charged). For example, in Lys for pH 3, 5, 7, and 9 the ZP values of Fe_2O_3-35 are 5, − 14, − 22, and − 27 mV (Fig. 6b), and for Fe_2O_3-120, they are 19, 0, − 20, and − 30 mV (Fig. 7b). The lowest agglomeration of both IOPNs in amino acids is reached at pH = 9: the d_{av} of Fe_2O_3-35 drops to 180 ± 20 nm (− 32 mV) compared with water 511 ± 20 nm (− 17 mV) (Fig. 6), whereas the minimum d_{av} of Fe_2O_3-120 is 263 ± 80 nm (− 38 mV) versus water—180 ± 69 nm (− 24 mV) (Fig. 7). Besides, the highest agglomeration stability of both particles is achieved in solutions of amino acids at pH = 9 as in water: ZP reaches − 27–− 38 mV compared with − 18 mV in water (Figs. 6b and 7b).

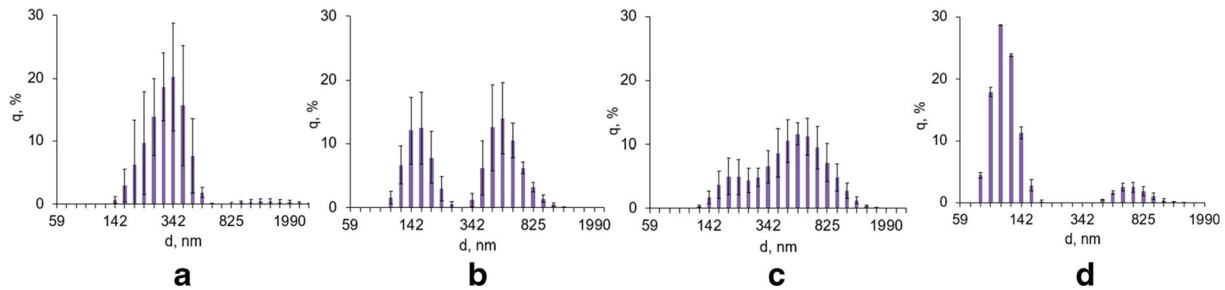

Fig. 4 The particle and agglomerate size distribution for Fe_2O_3-120. **a** pH = 3. **b** pH = 5. **c** pH = 7. **d** pH = 9

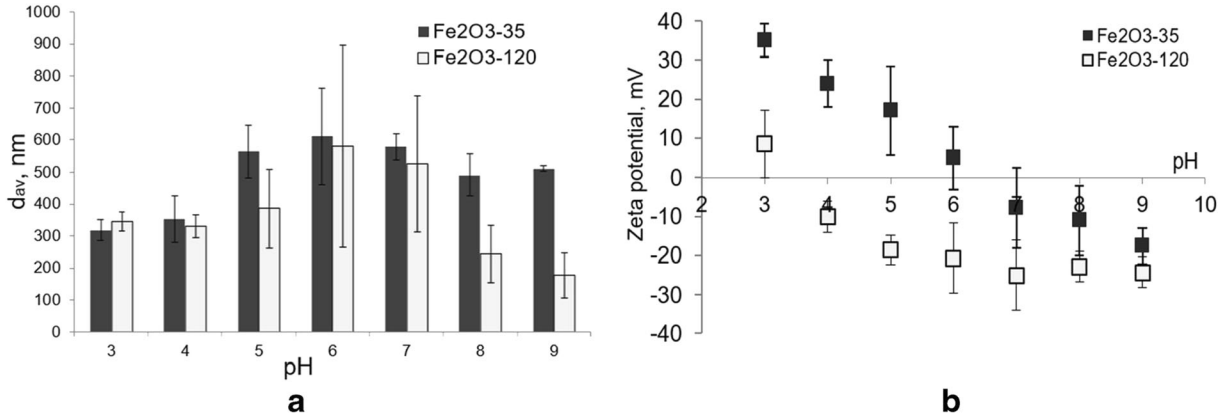

Fig. 5 The pH effect on the average size d_{av} (**a**) and zeta potential (**bs**) of Fe_2O_3-35 and Fe_2O_3-120 particles in hydrosols

The effect of particle size on the agglomeration state and stability of nanoparticle hydrosols

Although powders were produced by different methods, the surface chemistry of both particles was identical. The sample of Fe_2O_3-35 was annealed at 500 °C and included only hematite. In Fe_2O_3-120, small amounts Fe_3O_4 and Fe were mainly inside biggest particles. Therefore, we compared size effect on the agglomeration state and stability of nanoparticle hydrosols.

It has been experimentally shown that in spite of different particle size and fabrication conditions, the surface of Fe_2O_3 nanoparticles in amino acid solutions is charged positively at pH = 3. Moreover, the surface isoelectric point of both particles is in an acidic medium (pH ~ 4 for Fe_2O_3-35 (Fig. 6b) and pH ~ 5 for Fe_2O_3-120 particles (Fig. 7b). Low electrokinetic stability initiates the agglomeration of particles at pH = 3–5. The sizes of agglomerates exceed their sizes in water averagely by 2 times (1.9 and 2.6 times for Fe_2O_3-35 and Fe_2O_3-120, respectively, Figs. 6a and 7a). Also, the mutual tendency is that in the range of pH = 5–9, adding OH^- leads to a weaker agglomeration and the formation of more stable IONP hydrosols: at pH = 9, there are particles with minimum d_{av} and maximum charge (− 38 mV).

It has been found that the addition of amino acids to the hydrosols in acidic conditions causes different net charges depending on the initial particle size. Thus, the net charge of smaller particles is more negative (Fig. 6b), whereas the surface of bigger particles is more positively charged compared with water (Fig. 7b). For example, in Lys at pH = 3, the ZP values of Fe_2O_3-35 and Fe_2O_3-120 are 5.4 and 24 mV (Fig. 6b and 7b)

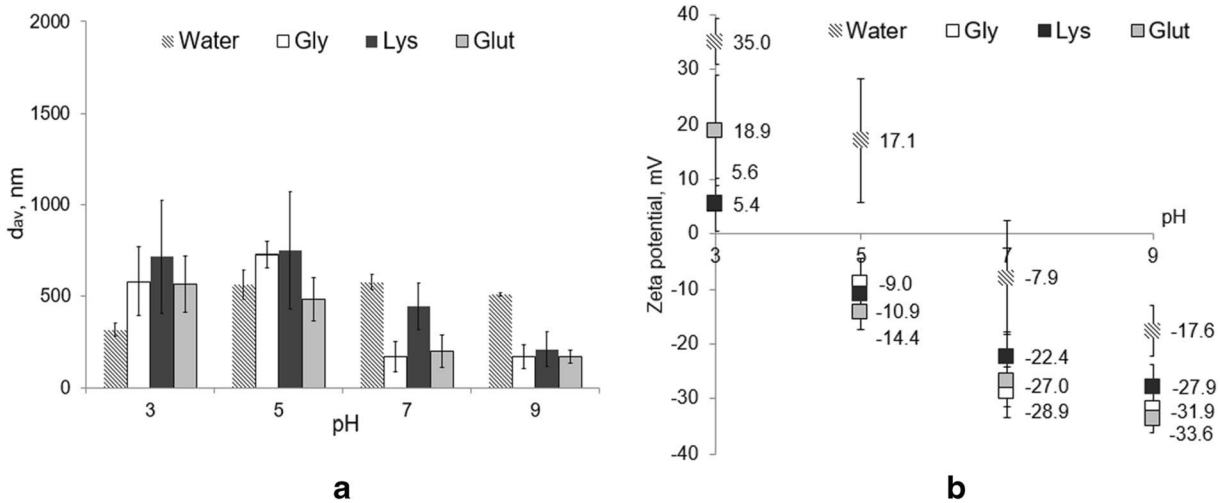

Fig. 6 The pH effect on the average size of agglomerates d_{av} (**a**) and zeta potential (**b**) of Fe_2O_3-35 particles in amino acid solutions

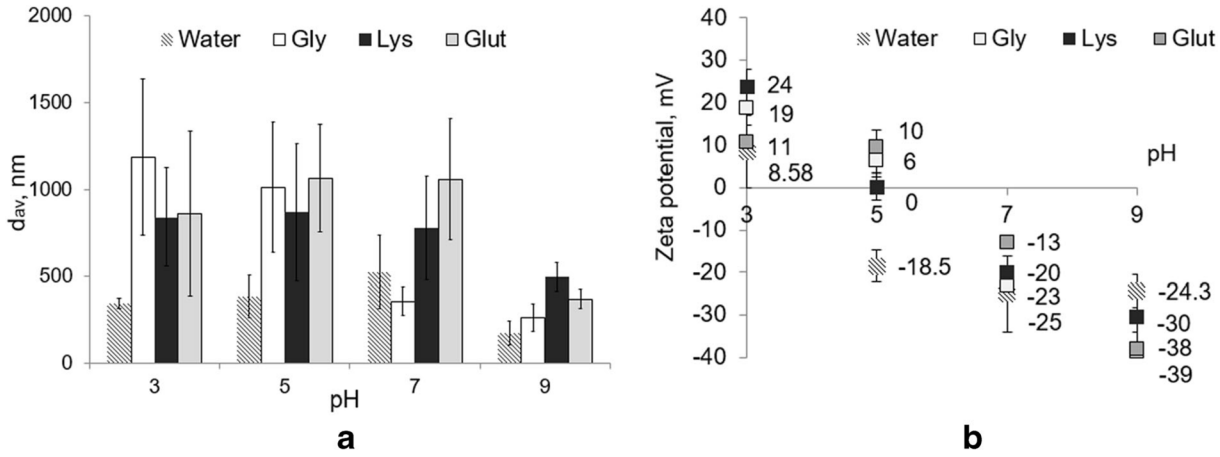

Fig. 7 The pH effect on the average size of agglomerates d_{av} (**a**) and zeta potential (**b**) of Fe_2O_3-120 particles in amino acid solutions

while in water, it is 35 and 9 mV, respectively (Fig. 5b). Apparently, different electrosurface properties are connected not only with the size (and, therefore, the surface adsorbing surfactants) but also with the surface quality state that is changing due to the conditions of fabrication. Probably, negatively charged COOH- anions are concentrated on the Fe_2O_3-35 surface with a higher positive charge and decreased ZP value. Meanwhile, positive NH_2^+ groups settle on the more negatively charged surface of Fe_2O_3-120 that leads to a higher ZP. In the alkaline medium, the concentration of OH^- obviously prevails over the influence of particle size.

If we estimate the agglomeration degree as the number of particles in an agglomerate, it may be concluded that regardless of the media, the agglomeration degree of IONPs increases for smaller particles. Indeed, for Fe_2O_3-120 and Fe_2O_3-35, the agglomeration degrees are, respectively, 5.4 and 6.8 in air, 1.5 and 14.6 in water (pH = 9), and − 1.4 and 5.1 in Gly (pH = 9).

The effect of acidity of amino acids on the particle agglomeration in hydrosol

Despite the different acidities of amino acids at their selected concentrations, particle behavior differs slightly in acidic media: at pH = 3–5, the size of the agglomerates in all surfactants exceeds d_{av} in water by 1.8–3.6 times (Figs. 6a and 7a). Despite the fact that at pH < 7, amino acid cations H_3N-CHR-COOH replace the protons concentrated on the particle surface, and the solvation shell grows significantly, the agglomeration is mostly caused by the surface charge close to the isoelectric point (Figs. 6b and 7b), which leads to particles sticking due to intermolecular Van der Waals interaction between particles.

It has been demonstrated that in surfactant solutions, isoelectric point of the IONPs remain in an acidic media even if it is shifted in the presence of all amino acids. The surface of the bare Fe_2O_3-35 and Fe_2O_3-120 particles has neutral charge at pH = 6.5 and pH = 3.5, respectively. Indeed, in surfactant solutions, regardless of the amino acid nature, isoelectric points of the Fe_2O_3-35 and Fe_2O_3-120 are at pH = 4 ± 0.2 and pH = 5 ± 0.2, respectively (Figs. 6b and 7b). However, α-amino acid nature affects isoelectric state of TiO_2 nanoparticle surfaces: glycine and lysine increase the pH of the isoelectric point from 6.1 to 6.4 and 7.1, respectively, whereas glutamic acid and serine decrease for the value of pH of neutrally charged particles to 5.4 and 4.4, respectively, as shown recently (Ustunol et al. 2019).

Furthermore, in all the prepared hydrosols at higher concentration of OH^- ions, the net charge of the particles goes towards negative values: for example, at pH 3, 5, 7, and 9, the ZP of Fe_2O_3-35 and Fe_2O_3-120 particles in Lys is 5, − 14, − 26, and − 32 mV (Fig. 6b) and 19, 0, − 20, and − 30 mV, respectively (Fig. 7b). This behavior could be explained by the presence of negatively charged $COOH^-$ ions, but in an acidic environment, the adsorption of functional groups is more associated with the particle nature, rather than with the amino acid nature. Due to the fact that the same trend is observed for hydrosols without surfactants, it can be concluded that under the chosen conditions, the influence of the pH has a greater impact on the agglomeration and stability of IONPs compared with amino acid nature.

Generally, with an increase of the pH from 3 to 9, all suspensions are characterized by particle size reduction: for example, in Gly at pH 3, 5, 7, and 9, d_{av} is 581, 725, 170, and 170 nm (Fig. 6a) and 1188, 1014, 358, and 263 nm (Fig. 7a) for Fe_2O_3-35 and Fe_2O_3-120, respectively. At the same time, the impact of pH on the agglomeration shows maximum in neutral surfactants. For example, when increasing the pH from 5 to 9, the d_{av} decreases in the series of Lys, Glut, and Gly by 1.8, 2.8, and 4.5 times (Fig. 7a). That is consistent, for example, with the study (Wang et al. 2011), wherein the solution of neutral amino acid arginine synthesized nanoparticles smaller than particles synthesized in a solution of a basic amino acid—lysine. Under the equal acid-basic conditions, the effect of amino acid acidity on the particle charge is not significant: for example, in Gly, Lys, and Glut, at pH = 5, the zeta potential of Fe_2O_3-120 is − 9, − 10, and − 14 mV (Fig. 6b).

Conclusion

In this work, we used iron oxide (III) nanoparticles synthesized by two different methods—pulsed laser ablation followed by annealing and electric explosion of a metallic conductor in air, with an average particle sizes of 35 and 120 nm and sizes of dry agglomerates of 240 and 660 nm (SEM data), respectively, in order to show the influence of pH and acidity of aliphatic amino acids (glycine, glutamine, and lysine) as surfactants on the agglomeration state and stability of particles in hydrosols. The analysis of particle size distributions obtained by the dynamic light scattering method showed that in hydrosols containing 0.01–0.1 wt% particles and 0.05 wt% of amino acids, there are both individual and agglomerated particles. The agglomeration degree and surface charge of particles highly depends on acid-basic conditions and the size of dry particles.

It has been shown that the agglomeration degree of Fe_2O_3-35 particles in the hydrosols without amino acids (only ultrasonic treatment) is almost unchanged at pH = 3–9, while the agglomeration of Fe_2O_3-120 particles is weakened only with an excess of OH^- ions. After adding amino acids, regardless of their acidity and initial particle size, the agglomeration degree of Fe_2O_3 particles at pH = 3 increases by 2 times compared with water (1.9 and 2.6 times for Fe_2O_3-35 and Fe_2O_3-120, respectively) and particles are positively charged. With the pH growth from 5 to 9, the particles disagglomerate in all surfactants. If we define the degree of pH effect as agglomerate size reduction, it can be seen that Gly-hydrosols are most susceptible to pH effect. Thus, with an increase of the pH from 5 to 9, the d_{av} decreases by 1.8 times in lysine (basic acid), 2.8 times in glutamine (acidic amino acid), and 4.5 times in glycine (neutral amino acid).

Furthermore, the lowest agglomeration stability of Fe_2O_3 particles has been found at pH = 3.5–6.5 due to a low net charge close to the surface isoelectric point. Besides, at pH ≤ 7, particle agglomeration stability is more connected with the particle nature or the fabrication conditions.

Due to insignificant contribution of surfactant acidity to the particle surface charge, it has been concluded that the pH have the prevailing impact on the particle agglomeration state and stability over the acidity of amino acids. As demonstrated, at pH = 9, the maximum disagglomeration of both particles is achieved: the size of Fe_2O_3-35 is 180 ± 20 nm (− 32 mV) compared with water 511 ± 20 nm (− 17 mV); for Fe_2O_3-120, the size is 263 ± 80 nm (− 38 mV) versus 180 ± 69 nm (− 24 mV) in water.

Based on the obtained results, it can be concluded that the agglomeration state and stability of Fe_2O_3 hydrosols in an acidic medium (pH = 3–5) are influenced by the pH and the initial size of the dry particles. To these factors, the influence of acidity of amino acids in a neutral medium is added, but in weak alkaline solution, stability is affected only by the pH.

According to the classification of nanoparticle suspensions by stability given in the study (Patel and Agrawal 2011), hydrosols obtained in this work can be classified as moderately (± 20–± 30 mV) at pH = 7 and highly stable (< ± 30 mV) at pH = 9 for both Fe_2O_3-35 and Fe_2O_3-120 nanoparticles in amino acid solutions. Stable particles tend to form smaller agglomerates which have higher mobility compared with bigger agglomerates. Indeed, agglomeration and stability of nanoparticles is extremely important in order to conceive and to predict the mobility, reactivity, and bio-environmental fate of nanoparticles. It has been proven that when nanomaterials enter complex biological environment, biomolecules are adsorbed to their surface, forming nanomaterial-corona complexes stabilizing nanoparticles (Palchetti et al. 2016). Due to the moderate stability of hydrosols achieved in neutral medium (− 29 mV), hematite nanoparticles may easily migrate in biological fluids which mostly have the pH between 7 and 7.5.

It is obvious that the properties of hematite nanoparticles are most sensitive to external factors in a weakly acidic medium (from 5 to 7) provoking the surface charge exchange and the size-depended orientation of the functional groups. Regarding the practical application of the results, it can be used to prepare hematite nanoparticle suspensions in an alkaline medium to ensure high electrokinetic stability of hydrosols. The large surface charge makes it possible to prevent the nanoparticle agglomeration throughout the analysis process that can last up to 60 min.

Acknowledgments X-ray analysis was carried out in the framework of Tomsk Polytechnic University Competitiveness Enhancement Program, Russia. Synthesis of Fe_2O_3-35 particles was carried out in the framework of Tomsk State University Competitiveness Enhancement Program.

Funding information The work was supported by the Ministry of Science and Education of the Russian Federation, Russian Fund for Basic Research (project # 15-03-06528_a), and in the framework of Increase Competitiveness Program of NUST "MISiS."

Compliance with ethical standards

Conflict of interest The authors declare that they have no conflict of interest.

References

Bao Y, Wen T, Samia ACS, Khandhar A, Krishnan KM (2015) Magnetic nanoparticles: material engineering and emerging applications in lithography and biomedicine. J Mater Sci 51(1):513–553. https://doi.org/10.1007/s10853-015-9324-2

Bhattacharya D, Sahu S, Banerjee I, Das M, Mishr D, Maiti TK, Pramanik P (2011) Synthesis, characterization, and in vitro biological evaluation of highly stable diversely functionalized superparamagnetic iron oxide nanoparticles. J Nanopart Res 13:4173–4188. https://doi.org/10.1007/s11051-011-0362-7

Biju CS, Raja DH, Padiyan DP (2014) Glycine assisted hydrothermal synthesis of α-Fe_2O_3 nanoparticles and its size dependent properties. Chem Phys Lett 610-611:103–107. https://doi.org/10.1016/j.cplett.2014.07.024

Cabrera D, Camarero J, Ortega D, Teran FJ (2015) Influence of the aggregation, concentration, and viscosity on the nanomagnetism of iron oxide nanoparticle colloids for magnetic hyperthermia. J Nanopart Res 17(121). https://doi.org/10.1007/s11051-015-2921-9

Cao H, Wang G, Warner JH, Watt AAR (2008) Amino-acid-assisted synthesis and size-dependent magnetic behaviors of hematite nanocubes. Appl Phys Lett 92:013110. https://doi.org/10.1063/1.2830699

Chaudhari NK, Kim M, Bae T, Yu J (2013) Hematite (α-Fe_2O_3) nanoparticles on vulcan carbon as an ultrahigh capacity anode material in lithium ion battery. Electrochim Acta 114:60–67. https://doi.org/10.1016/j.electacta.2013.09.169

De Sousa ME, Fernández van Raap MB, Rivas PC, Mendoza Zélis P, Girardin P, Pasquevich GA, Alessandrini JL, Muraca D, Sánchez FH (2013) Stability and relaxation mechanisms of citric acid coated magnetite nanoparticles for magnetic hyperthermia. J Phys Chem 117:5436–5445. https://doi.org/10.1021/jp311556b

Demangeat E, Pedrot M, Dia A, Bouhnik-le-Coz M, Grasset F, Hanna K, Kamagatec M, Cabello-Hurtado F (2018) Colloidal and chemical stabilities of iron oxide nanoparticles in aqueous solutions: the interplay of structural, chemical and environmental drivers. Environ Sci Nano 5:992–1001. https://doi.org/10.1039/C7EN01159H

Doyen M, Goole J, Bartik K, Bruylants G (2016) Amino acid induced fractal aggregation of gold nanoparticles: why and how. J Colloid Interface Sci 464:160–166. https://doi.org/10.1016/j.jcis.2015.11.017

Farre M, Gajda-Schrantz K, Kantiani L, Barcelo D (2009) Ecotoxicity and analysis of nanomaterials in the aquatic environment. Anal Bioanal Chem 393:81–95. https://doi.org/10.1007/s00216-008-2458-1

Favela-Camacho SE, Samaniego-Benitez EJ, Godinez-Garcia A, Aviles-Arellano LM, Perez-Robles JF (2019) How to decrease the agglomeration of magnetite nanoparticles and increase their stability using surface properties. Colloid Surface A 574:29–35. https://doi.org/10.1016/j.colsurfa.2019.04.016

Gao J, Wei W, Shi M, Han H, Lu J, Xie J (2016) A controlled solvethermal approach to synthesize nanocrystalline iron oxide for Congo red adsorptive removal from aqueous solutions. J Mater Sci 51:4481–4494. https://doi.org/10.1007/s10853-016-9760-7

Holbrook RD, Galyean AA, Gorham JM, Herzing A, Pettibone J (2015) Overview of nanomaterial characterization and metrology. Frontiers of Nanoscience 8:47–87. https://doi.org/10.1016/b978-0-08-099948-7.00002-6

Ingram DR, Kotsmar C, Yoon KY, Shao S, Huh C, Bryant SL, Milner TE, Johnston KP (2010) Superparamagnetic nanoclusters coated with oleic acid bilayers for stabilization of emulsions of water and oil at low concentration. J Colloid Interface Sci 351:225–232. https://doi.org/10.1016/j.jcis.2010.06.048

ISO 13099-2:2012, Colloidal system. Methods for zeta potential determination. Part 2: Optical methods, June 2012

Jiang J, Oberdörster G, Biswas P (2009) Characterization of size, surface charge, and agglomeration state of nanoparticle dispersions for toxicological studies. J Nanopart Res 11(1):77–89. https://doi.org/10.1007/s11051-008-9446-4

Kandori K, Sakai M, Inoue S, Ishikawa T (2006) Effects of amino acids on the formation of hematite particles in a forced hydrolysis reaction. J Colloid Interface Sci 293:108–115. https://doi.org/10.1016/j.jcis.2005.06.029

Kast CE, Schnurch AB (2001) Thiolated polymers-thiomers: development, in vitro evaluation of chitosan-thioglycolic acid conjugates. Biomaterials 22:2345–2352. https://doi.org/10.1016/s0142-9612(00)00421-x

Li J, Wang S, Shi X, Shen M (2017) Aqueous-phase synthesis of iron oxide nanoparticles and composites for cancer diagnosis

and therapy. Adv Colloid Interf Sci 249:374–385. https://doi.org/10.1016/j.cis.2017.02.009

Li W, Liu D, Wu J, Kim C, Fortner JD (2014) Aqueous aggregation and surface deposition processes of engineered superparamagnetic iron oxide nanoparticles for environmental applications. Environ Sci Technol 48:11892–11900. https://doi.org/10.1021/es502174p

Lin C-L, Lee C-F, Chiu W-Y (2005) Preparation and properties of poly(acrylic acid) oligomer stabilized superparamagnetic ferrofluid. J Colloid Interface Sci 291:411–420. https://doi.org/10.1016/j.jcis.2005.05.023

Lin D, Cai P, Peacock CL, Wu Y, Gao C, Peng W, Huang Q, Liang W (2018) Towards a better understanding of the aggregation mechanisms of iron (hydr)oxide nanoparticles interacting with extracellular polymeric substances: role of pH and electrolyte solution. Sci Total Environ 645:372–379. https://doi.org/10.1016/j.scitotenv.2018.07.136

Liu JF, Zhao ZS, Jiang GB (2008) Coating Fe_3O_4 magnetic nanoparticles with humic acid for high efficient removal of heavy metals in water. Environ Sci Technol 42:6949–6954. https://doi.org/10.1021/es800924c

Lucas IT, Durand-Vidal S, Dubois E, Chevalet J, Turq P (2007) Surface charge density of maghemite nanoparticles: role of electrostatics in the proton exchange. J Phys Chem C 111: 18568–18576. https://doi.org/10.1021/jp0743119

Majewski P, Thierry B (2007) Functionalized magnetite nanoparticles – synthesis, properties, and bio-applications. Crit Rev Solid State 32(3–4):203–215. https://doi.org/10.1080/10408430701776680

Mohammed L, Gomaa HG, Ragab D and Zhu J (2017) Magnetic nanoparticles for environmental and biomedical applications: a review. Particuology 30:1–1. 10.1016/j.partic.2016.06.001, 14

Mohapatra S, Pramanik N, Mukherjee S, Ghosh SK, Pramanik P (2007) A simple synthesis of amine-derivatised superparamagnetic iron oxide nanoparticles for bioapplications. J Mater Sci 42:7566–7574. https://doi.org/10.1007/s10853-007-1597-7

Morgan LJ, Ananthapadmanabhan K, Somasundaran P (1986) Oleate adsorption on hematite: problems and methods. Int J Miner Process 18:139–152. https://doi.org/10.1016/0301-7516(86)90012-8

Nagajyothi PC, Pandurangan M, Kim DH, Sreekanth TVM, Shim J (2017) Green synthesis of Iron oxide nanoparticles and their catalytic and in vitro anticancer activities. J Clust Sci 28:245–257. https://doi.org/10.1007/s10876-016-1082-z

Parida P, Lolage M, Angal A, Rautaray D (2017) Iron oxide nanoparticles to remove arsenic from water. Nanoscience in Food and Agriculture 4:279–299. https://doi.org/10.1007/978-3-319-53112-0_10

Palchetti S, Pozzi D, Mahmoudi M, Caracciolo G (2016) Exploitation of nanoparticle–protein corona for emerging therapeutic and diagnostic applications. J Mater Chem B 4(25):4376–4381. https://doi.org/10.1039/c6tb01095d

Patel VR, Agrawal YK (2011) Nanosuspension: an approach to enhance solubility of drugs. J Adv Pharm Technol Res 2:81–87. https://doi.org/10.4103/2231-4040.82950

Ramos AP (2017) Dynamic light scattering applied to nanoparticle characterization. In: Alessandra L (ed) Nanocharacterization techniques, Elsiver, pp 99–110

Rasmussen K, Rauscher H, Mech A et al (2018) Physico-chemical properties of manufactured nanomaterials - characterisation and relevant methods. An outlook based on the OECD testing programme. Regul Toxicol Pharmacol 92:8–28. https://doi.org/10.1016/j.yrtph.2017.10.019

Ren X, Chen H, Yang V, Sun D (2014) Iron oxide nanoparticle-based theranostics for cancer imaging and therapy. Front Chem Sci Eng 8(3):253–264. https://doi.org/10.1007/s11705-014-1425-y

Schnurch AB, Hornof M, Guggi D (2004) Thiolated chitosans. Eur J Pharmacol Biopharm 57:9–17. https://doi.org/10.1016/s0939-6411(03)00147-4

Shen W-Z, Cetinel S, Sharma K, Borujeny ER, Montemagno C (2017) Peptide-functionalized iron oxide magnetic nanoparticle for gold mining. J Nanopart Res 19:74. https://doi.org/10.1007/s11051-017-3752-7

Svetlichnyi VA, Shabalina AV, Lapin IN, Goncharova DA, Velikanov DA, Sokolov AE (2018) Study of iron oxide magnetic nanoparticles obtained via pulsed laser ablation of iron in air. Appl Surf Sci 462:226–236. https://doi.org/10.1016/j.apsusc.2018.08.116

Talbot D, Abramson S, Griffete N, Bée A (2018) pH-sensitive magnetic alginate/γ-Fe2O3 nanoparticles for adsorption/desorption of a cationic dye from water. Journal of Water Process Engineering 25:301–308. https://doi.org/10.1016/j.jwpe.2018.08.013

Tartaj P, del Puerto Morales M, Veintemillas-Verdaguer S, Gonz lez-Carre T, Serna CJ (2003) The preparation of magnetic nanoparticles for applications in biomedicine. J Phys D: Appl Phy 36(13):R182–R197. https://doi.org/10.1088/0022-3727/36/13/202

Teja AS, Holm LJ (2002) Supercritical fluid technology in materials science and engineering: synthesis, properties, and applications. Elsevier, pp 327–349

Teja AS, Koh P-Y (2009) Synthesis, properties, and applications of magnetic iron oxide nanoparticles. Prog Cryst Growth & Charact 55:22–45. https://doi.org/10.1016/j.pcrysgrow.2008.08.003

Ustunol IB, Gonzalez-Pech NI, Grassian VH (2019) pH-dependent adsorption of α-amino acids, lysine, glutamic acid, serine and glycine, on TiO_2 nanoparticle surfaces. J Colloid Interf Sci accepted 554:362–375. https://doi.org/10.1016/j.jcis.2019.06.086

Wang GH, Li WC, Jia K, Lu AH, Feyen M, Spliethoff B, Schüth F (2011) A facile synthesis of shape- and size-controlled α-Fe_2O_3 nanoparticles through hydrothermal method. Nano 5: 469–479. https://doi.org/10.1142/s1793292011002846

Wu D, Liu P, Wang T, Chen X, Yang L, Jia D (2018) Amino acid-assisted synthesis of Fe2O3/nitrogen doped graphene hydrogels as high performance electrode material. Electrochim Acta 283:1858–1870. https://doi.org/10.1016/j.electacta.2018.07.103

Xu XQ, Shen H, Xu JR, Xie MQ, Li XJ (2006) The colloidal stability and core-shell structure of magnetite nanoparticles coated with alginate. Appl Surf Sci 253:2158–2164. https://doi.org/10.1016/j.apsusc.2006.04.015